

Article

Photoelectrocatalytic Properties of a Ti-Modified Nanocrystalline Hematite Film Photoanode

Vitali A. Grinberg , Victor V. Emets , Natalia A. Mayorova, Aleksey A. Averin and Andrei A. Shiryaev 

Frumkin Institute of Physical Chemistry and Electrochemistry, Russian Academy of Sciences, Leninsky Prospekt 31, Building 4, 119071 Moscow, Russia

* Correspondence: vitgreen@mail.ru

Abstract: Photoelectrocatalytic oxidation of methanol, ethylene glycol, glycerol, and 5,6,7,8-tetrahydro-2-naphthol on thin-film nanocrystalline hematite electrodes fabricated by electrochemical deposition and promoted with spin-coated titanium has been studied. It is shown that the modification of hematite transforms it into material exhibiting high activity in the photoelectrochemical process of substrate oxidation upon illumination with light in the visible region of the spectrum. The highest activity is observed in the reaction of photoelectrocatalytic oxidation of glycerol. Results of intensity-modulated photocurrent spectroscopy (IMPS) suggest that the effect is due to an increased rate of charge transfer in the process of photoelectro-oxidation and efficient suppression of the recombination of generated electron-hole pairs. Therefore, thin-film photoanodes based on modified hematite are promising for practical application in the photooxidation of glycerol, a by-product of biofuel production, as well as in the photoelectrochemical degradation of other organic pollutants, including those formed during the production of pharmaceuticals.

Keywords: hematite photoanode titanium-promoted; electrochemical deposition; photoelectrocatalytic oxidation; methanol; ethylene glycol; glycerol; 5,6,7,8-tetrahydro-2-naphthol



Citation: Grinberg, V.A.; Emets, V.V.; Mayorova, N.A.; Averin, A.A.; Shiryaev, A.A. Photoelectrocatalytic Properties of a Ti-Modified Nanocrystalline Hematite Film Photoanode. *Catalysts* **2022**, *12*, 1243. <https://doi.org/10.3390/catal12101243>

Academic Editors: Nicolas Alonso-Vante and Bin Luo

Received: 6 September 2022

Accepted: 13 October 2022

Published: 15 October 2022

Publisher's Note: MDPI stays neutral with regard to jurisdictional claims in published maps and institutional affiliations.



Copyright: © 2022 by the authors. Licensee MDPI, Basel, Switzerland. This article is an open access article distributed under the terms and conditions of the Creative Commons Attribution (CC BY) license (<https://creativecommons.org/licenses/by/4.0/>).

1. Introduction

Pollution of water resources with organic substances due to industrial and agricultural activities is a serious environmental problem. Growing production of biodiesel leads to massive formation of large amounts of glycerol, a by-product of this process [1,2]. In this regard, transformation of glycerol into useful raw material is of considerable ecological importance. Various value-added products are obtained from glycerol, including acrylic [3], lactic [4,5], and glyceric acids, dihydroxyacetone, hydroxypyruvic and tartronic acids [6–8]. The decomposition of glycerol by pyrolysis and steam reforming requires thermal energy with concomitant environmental pollution. An increasing problem is also the growing pollution of the aquatic environment with difficult-to-oxidize products of the pharmaceutical industry, in particular antibiotics, hormonal drugs, etc., which requires the development of new methods for their degradation.

In recent decades, considerable efforts have been directed towards photoelectrochemical oxidation, i.e., transformation of organic substances using UV-Vis illumination [9–12]. As a rule, efficient photoelectrochemical oxidation using semiconductor electrodes requires high chemical stability during reactions, appropriate position of the absorption band, selectivity for substrate oxidation, and a low-cost photoanode [10].

As a promising alternative to traditional titanium dioxide photoanodes, zinc oxide (ZnO), which is characterized by higher absorption coefficient, electron mobility, nontoxicity, and low cost, is considered [11]. The possibility of photoelectrochemical oxidation of glycerol with the generation of glyceric acid on a cobalt-modified zinc oxide photoanode was shown in [13], where UV light was used.

Hematite $\alpha\text{-Fe}_2\text{O}_3$ is a semiconductor with a relatively small band gap (2.1–2.2 eV) and, therefore, can be photoexcited by photons with energies in the visible region of the spectrum [14,15]. This material is also characterized by low cost, nontoxicity, and good chemical stability in most aqueous solutions at $\text{pH} > 3$ [16,17], making it a promising material for the photoelectrocatalytic decomposition of water and organic pollutants [18–22]. In [23] the authors studied photoelectrochemical degradation of methanol in an aqueous solution on a thin-film hematite photoelectrode obtained by the sol-gel method and modified with titanium, cobalt, and bismuth. Illumination using photons from the visible part of the spectrum was employed. It was shown that simultaneous modification of Fe_2O_3 by titanium and cobalt increases selectivity of the photoanode with respect to the photoelectrooxidation of methanol from an aqueous solution.

The published data on the photoelectrocatalytic activity of modified hematite in aqueous solutions vary greatly. Furthermore, the photoconversion of hematite thin films is still insufficient due to the short diffusion length of charge carriers, low absorption coefficient, and high rate of electron-hole recombination. In the present work, we investigate the effect of promotion of electrodeposited hematite films with small amounts of titanium on its photoelectrocatalytic activity. Following [23], one may expect that such promotion will positively affect both the efficiency of charge separation and the rate constant of transfer. We report photoelectrocatalytic activity of Ti-modified hematite films upon visible light illumination in the process of methanol, ethylene glycol, glycerol, and 5,6,7,8-tetrahydro-2-naphthol oxidation. In addition, the effect of chemical structure of organic depolarizer on recombination processes is investigated. To the best of our knowledge, systematic studies of photoelectrochemical degradation of mono-, di-, and trihydric alcohols on semiconductor photoanodes have not yet been performed. Presumably, the photoelectrochemical activity of the latter will depend on the chemical structure of alcohols and on their competition with water molecules on the surface of a film photoanode during photoelectrooxidation. Similarly, there are no published studies of photoelectrochemical degradation of 5,6,7,8-tetrahydro-2-naphthol, a model compound for revealing reactivity of phenolic fragments of steroid hormones upon their removal from an aqueous medium. It should be noted that in this work, we did not intend to study the composition of the products of photoelectrocatalytic oxidation of substrates. This will be the subject of a subsequent separate study.

2. Results and Discussion

2.1. X-ray Diffraction (XRD), Raman and UV–Vis Spectroscopy

Figure 1 shows X-ray diffraction patterns of the conductive glass substrate and prepared photoanode samples from the original and titanium-modified hematite. The diffraction pattern of the glass-ceramic substrate is dominated by tin oxide reflections. Peaks in patterns of the samples unambiguously indicate the presence of rhombohedral $\alpha\text{-Fe}_2\text{O}_3$ particles (ICDD card 33-0664). Sample-dependent intensity variations of corresponding reflections can be attributed to texture effects (preferential alignment of grains in a given crystallographic direction). Similar to results of [24], in the samples (2) and (3) the hematite crystallites are preferentially oriented in the (110) direction, implying that, in a significant fraction of crystallites, the (001) basal plane is perpendicular to the substrate. This orientation facilitates the transfer of a photogenerated hole [25]. The size of hematite crystallites was calculated by independent methods (Scherrer and Williamson–Hall) which gave matching values. In both samples the grain size is 26–27 nm. Titanium compounds were not detected.

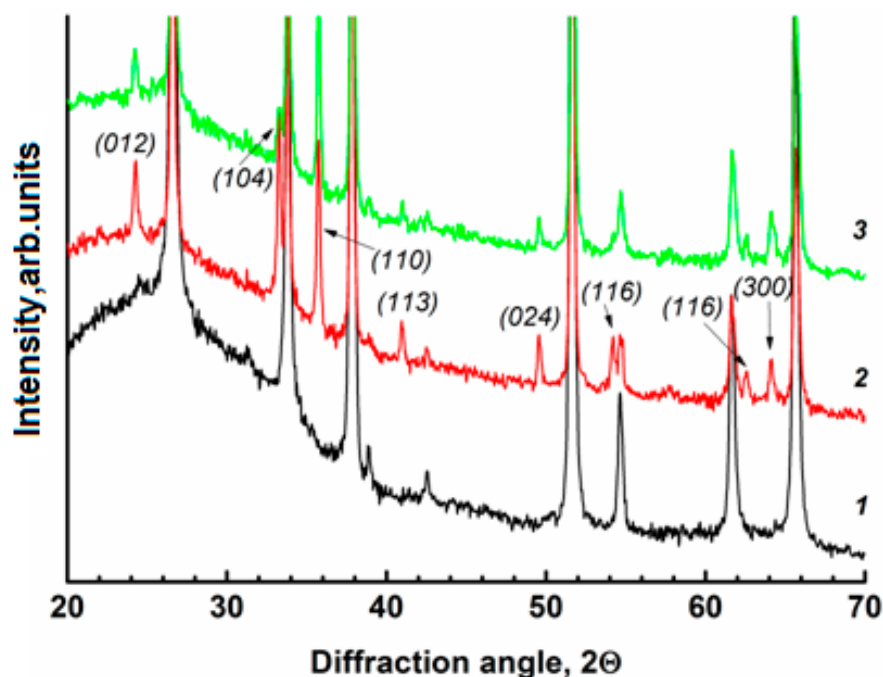


Figure 1. X-ray diffraction patterns of the samples: (1) conductive glass F:SnO₂ (FTO); (2) Fe₂O₃/FTO; (3) Ti⁴⁺/Fe₂O₃/FTO. The curves are displaced vertically for clarity. Diffraction peaks of hematite (α -Fe₂O₃) are marked (ICDD card 33-0664).

However, Raman spectra (Figure 2) clearly indicate the presence of anatase (a TiO₂ polymorph) manifested by characteristic peak at 144 cm⁻¹ and some other features [23]. One can assume the formation of a heterojunction TiO₂/Fe₂O₃. However, a shift of hematite Raman peaks of the Ti⁴⁺/Fe₂O₃/FTO sample relative to α -Fe₂O₃ reference likely indicates the formation of titanium solid solution. It is known that titanium oxide is readily soluble in iron oxide up to 20 mol.% [26]. The absence of the anatase X-ray reflections may be explained by their small volume fraction and/or poor crystallinity.

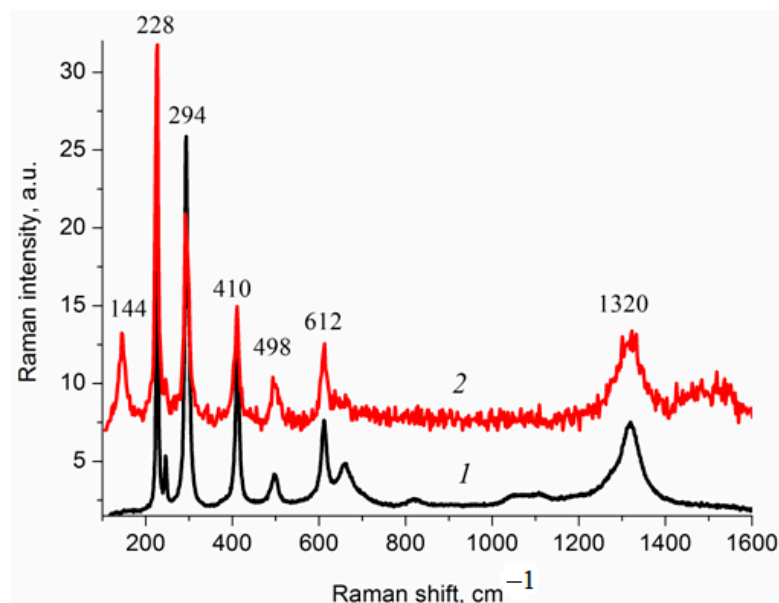
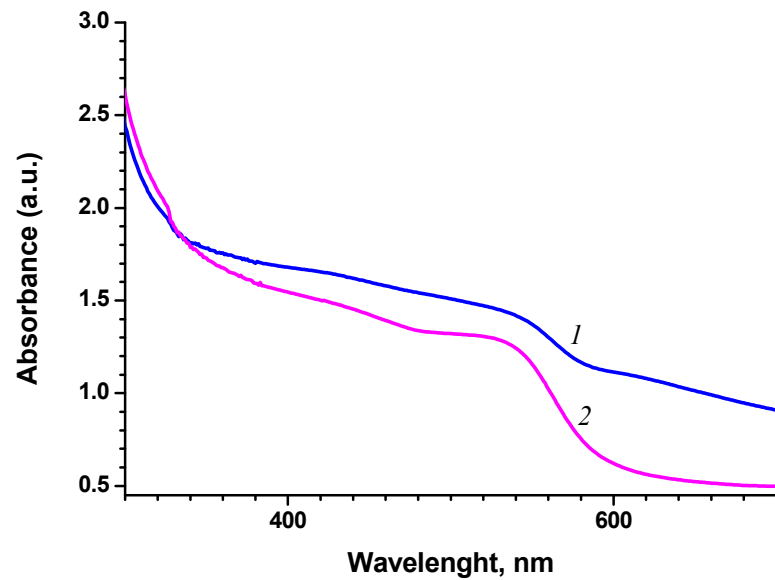


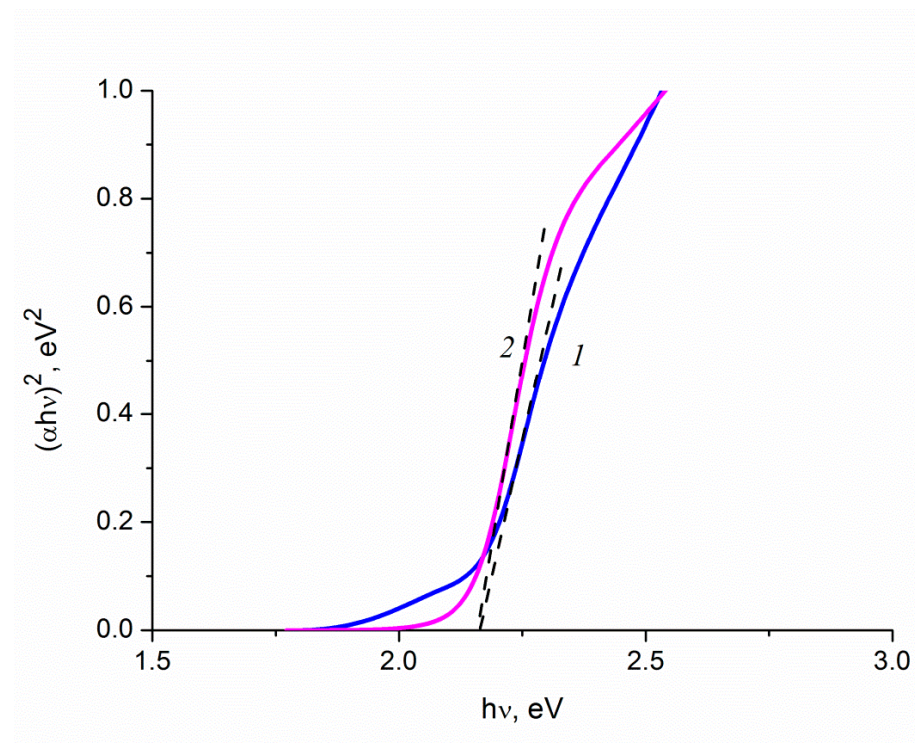
Figure 2. Raman spectra of photoanode samples: (1) Fe₂O₃/FTO; (2) Ti⁴⁺/Fe₂O₃/FTO. The curves are displaced vertically for clarity.

The absorption spectra of the Fe₂O₃/FTO and Ti⁴⁺/Fe₂O₃/FTO film samples are shown in Figure 3a. To maintain dependence on T_{auc} , in order to eliminate the contribution

associated with the film thickness, the curves shown in Figure 3a were normalized to [0, 1]. The direct band gap (E_g) was obtained by extrapolation of the linear part of the photon energy dependence of the function $(\alpha h\nu)^2$ [27,28] to the energy axis (Figure 3b). As can be seen from Figure 3b, the modification of Fe_2O_3 with titanium does not affect the band gap energy, which is close to 2.2 eV for the studied samples.



(a)



(b)

Figure 3. Absorption spectra of film photoanodes: (1) $\text{Fe}_2\text{O}_3/\text{FTO}$; (2) $\text{Ti}^{4+}/\text{Fe}_2\text{O}_3/\text{FTO}$ (a) and dependence of $(\alpha h\nu)^2$ on photon energy $h\nu$ for film photoanodes: (1) $\text{Fe}_2\text{O}_3/\text{FTO}$; (2) $\text{Ti}^{4+}/\text{Fe}_2\text{O}_3/\text{FTO}$ (b).

The structure and morphology of the initial electrodeposited α - Fe_2O_3 films, as well as their optical properties, correlate well with the literature data [29]. Microphotographs of the surface of titanium-doped hematite films (Figure 4) demonstrate that the films are homogeneous, dense and contain some defects.

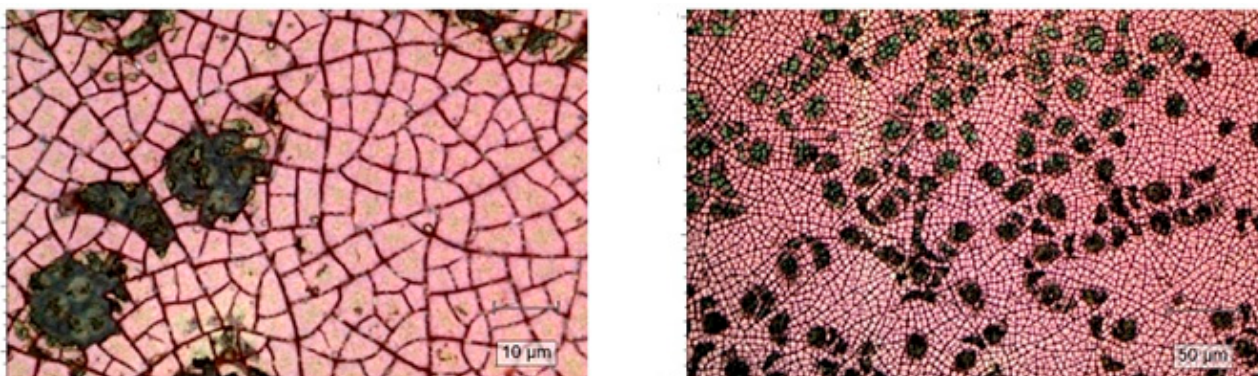


Figure 4. Micrographs of titanium-promoted hematite film samples at different magnification.

2.2. Influence of the Modifying Component on the Photoelectrocatalytic Oxidation of Water, Methanol, Ethylene Glycol and Glycerol

Preliminary experiments showed that promotion of the synthesized hematite films with a small amount of titanium dioxide leads to ~8-fold increase in the water oxidation photocurrent at the potential 0.4 V vs. Ag (Figure 5). This can be explained by an increase in the density of surface states of the photoanode upon modification with titanium [26]. This improves the efficiency of charge transfer in the process of photoelectrocatalytic oxidation of water molecules. It was also of interest to study the photoelectro-oxidation of other depolarizers on this photoanode.

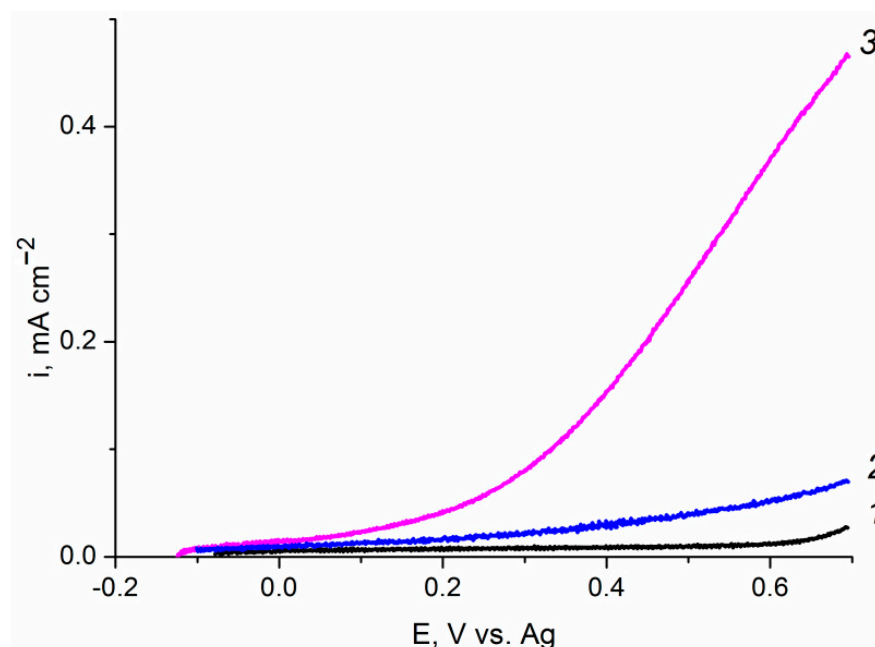


Figure 5. Current-voltage characteristics of (1, 3) $\text{Ti}^{4+}/\text{Fe}_2\text{O}_3/\text{FTO}$ and (2) $\text{Fe}_2\text{O}_3/\text{FTO}$ film photoanodes in aqueous solutions of 0.1 M KOH obtained in: (1) dark conditions; (2, 3) under visible light illumination with a power density of 100 mW cm^{-2} .

The polarization curves of photoelectro-oxidation of methanol, ethylene glycol, and glycerol on a $\text{Ti}^{4+}/\text{Fe}_2\text{O}_3/\text{FTO}$ film photoanode are shown in Figure 6. For each of the three

organic depolarizers, a well-pronounced wave of direct photoelectrochemical oxidation is observed. It is shifted to the cathodic side compared to the curve in background solution. A significant dependence of the photocurrent on the chemical nature of the depolarizer is observed. At a photoanode potential of 0.4 V vs. Ag electrode, the photocurrent in solutions with the addition of 20% methanol, ethylene glycol, or glycerol increases by factors of 2.4, 4.4, and 6, respectively, compared with the value in a 0.1 M KOH solution. An increase in the number of OH groups in an alcohol molecule is accompanied by a shift in the currentless potential and the entire polarization curve of the photocurrent towards the cathode side. The results obtained indicate an increase in the rate of photoelectro-oxidation in the series $\text{H}_2\text{O} < \text{CH}_3\text{OH} < \text{C}_2\text{H}_4(\text{OH})_2 < \text{C}_3\text{H}_5(\text{OH})_3$. This can be explained by the influence of the chemical nature of the depolarizer both on the rate constant of photoelectro-oxidation and on recombination processes on the surface states of the promoted hematite photoanode.

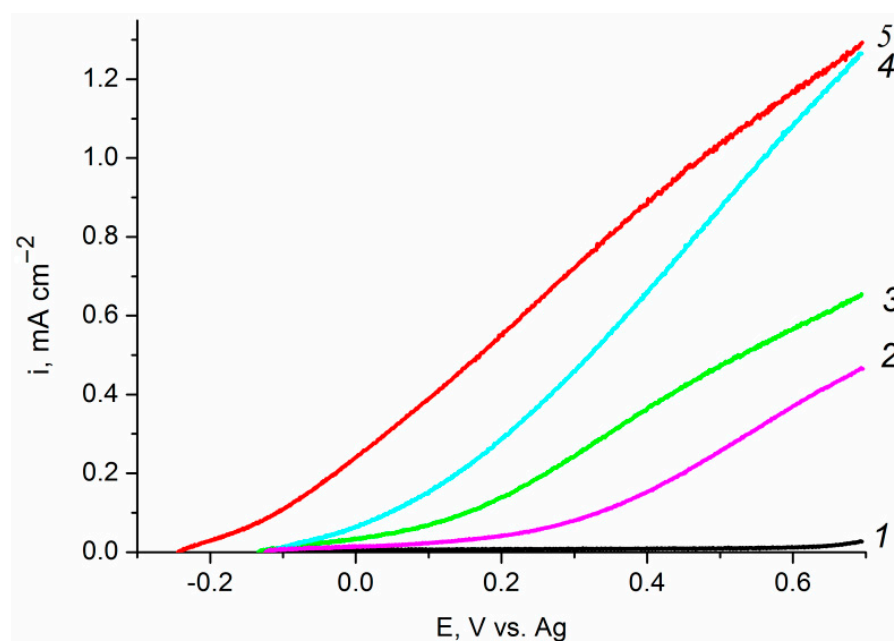


Figure 6. Polarization curves of a $\text{Ti}^{4+}/\text{Fe}_2\text{O}_3/\text{FTO}$ film photoanode measured: (1) in dark conditions, and (2–5) under visible light illumination with a power density of 100 mW cm^{-2} in aqueous solutions of (2) 0.1 M KOH; (3) 0.1 M KOH + 20% CH_3OH ; (4) 0.1 M KOH + 20% $\text{C}_2\text{H}_4(\text{OH})_2$; and (5) 0.1 M KOH + 20% $\text{C}_3\text{H}_5(\text{OH})_3$.

The presence of recombination losses is evidenced by the shape of the photocurrent transients shown in Figure 7. It can be seen that in a 0.1 M KOH solution, switching the light “on” and “off” leads to sharp jumps in the photocurrent, which, during the photoelectrocatalytic oxidation of water molecules, quickly drops to a stationary value (Figure 8, curve 1) due to partial recombination of photogenerated electron-hole pairs. The indicated current jumps, and, consequently, the associated recombination losses, decrease significantly when 20% CH_3OH is added to the background solution (Figure 7, curve 2), and practically disappear upon addition of 20% $\text{C}_3\text{H}_5(\text{OH})_3$ (Figure 7, curve 3). The main contribution to recombination losses in the process of photoelectrocatalytic oxidation of substrates on a $\text{Ti}^{4+}/\text{Fe}_2\text{O}_3/\text{FTO}$ film photoanode is made by surface states (SS), while the role of bulk recombination is much smaller [26].

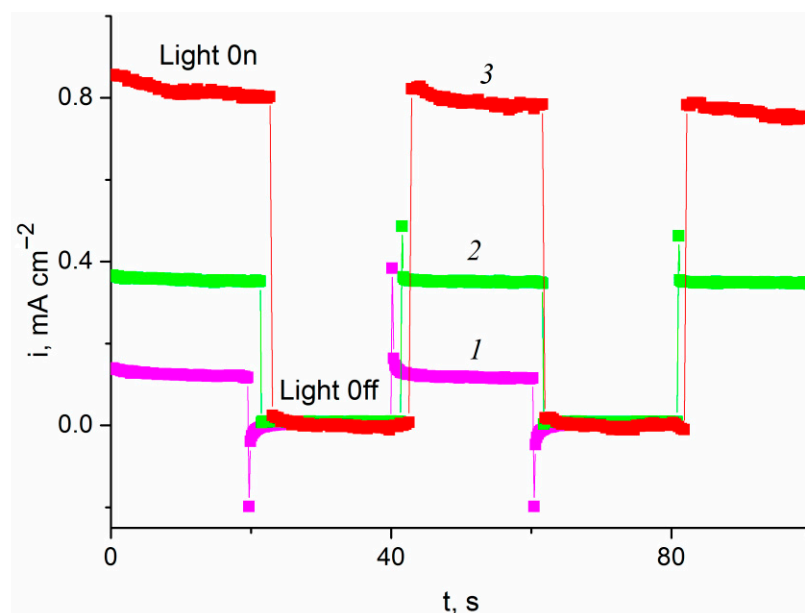


Figure 7. Photocurrent transients obtained at $E = 0.4$ V on the film photoanode $\text{Ti}^{4+}/\text{Fe}_2\text{O}_3/\text{FTO}$ in dark conditions and under visible light illumination with a power of 100 mW cm^{-2} in aqueous solutions: (1) 0.1 M KOH; (2) 0.1 M KOH + 20% CH_3OH ; (3) 0.1 M KOH + 20% $\text{C}_3\text{H}_5(\text{OH})_3$.

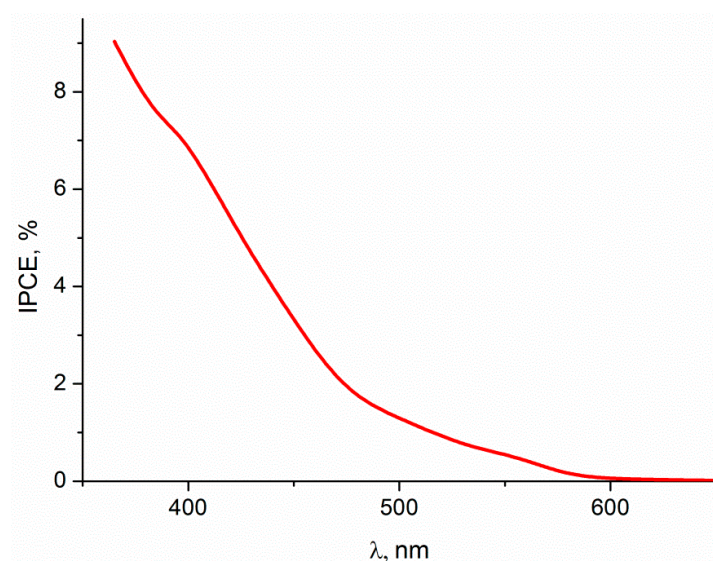


Figure 8. IPCE% spectrum for a $\text{Ti}^{4+}/\text{Fe}_2\text{O}_3/\text{FTO}$ photoanode in an aqueous solution of 0.1 M KOH + 20% $\text{C}_3\text{H}_5(\text{OH})_3$.

2.3. Estimation of Recombination Losses during Photoelectro-Oxidation of Water, Methanol, Ethylene Glycol and Glycerol

Dependence of the incident photon-to-current conversion efficiency (IPCE%) of a $\text{Ti}^{4+}/\text{Fe}_2\text{O}_3/\text{FTO}$ film photoanode on the wavelength of monochromatic light in an aqueous solution of 0.1 M KOH + 20% $\text{C}_3\text{H}_5(\text{OH})_3$ is shown in Figure 8. It can be seen that the photoactivity manifests itself in the wavelength range of 350–600 nm. Comparison of Figures 8 and 3a shows a good correlation between the IPCE% spectrum and the absorption spectrum for this sample (Figure 3a, curve 2). To quantify the recombination losses during the photoelectro-oxidation of water, methanol, ethylene glycol, and glycerol on a titanium-promoted hematite electrode, the method of Intensity-modulated photocurrent spectroscopy (IMPS) was used [30–33]. To record the IMPS dependences, we used monochromatic illumination with a wavelength of 452 nm in the visible region, which provides a fairly high value of IPCE% (Figure 8).

The IMPS spectra for a $\text{Ti}^{4+}/\text{Fe}_2\text{O}_3/\text{FTO}$ film photoanode measured during the photoelectro-oxidation of water, methanol, and glycerol are presented in Figure 9.

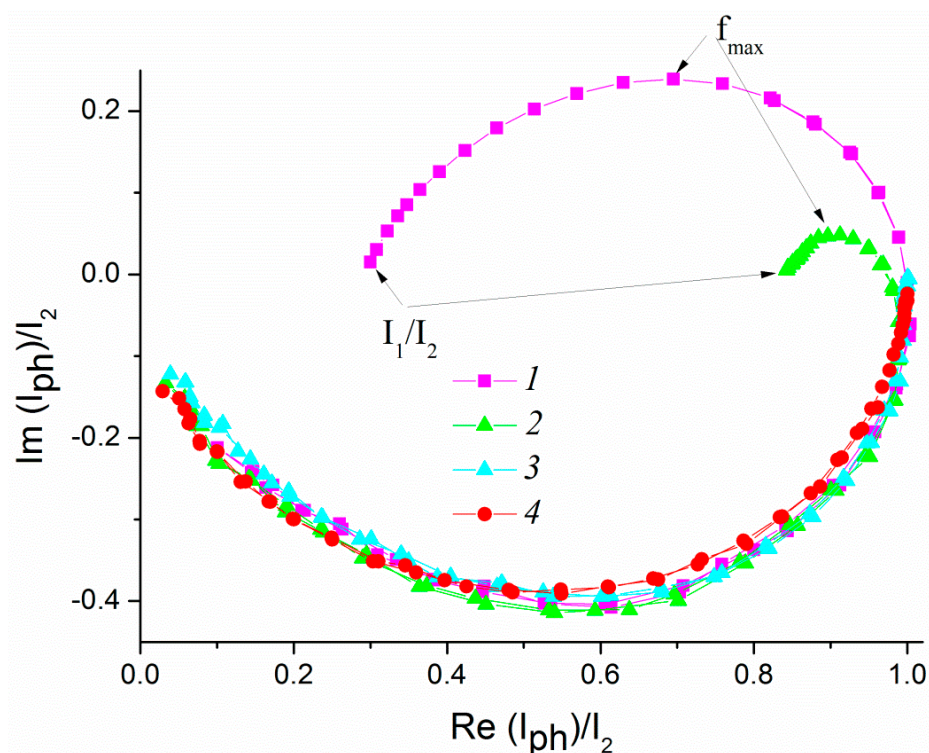


Figure 9. Normalized IMPS dependences for a $\text{Ti}^{4+}/\text{Fe}_2\text{O}_3/\text{FTO}$ film photoanode illuminated with monochromatic light 452 nm at the illumination power density 14 mW cm^{-2} , obtained at a potential of 0.4 V in aqueous solutions of: (1) 0.1 M KOH; (2) 0.1 M KOH + 20% CH_3OH ; (3) 0.1 M KOH + 20% $\text{C}_2\text{H}_4(\text{OH})_2$; (4) 0.1 M KOH + 20% $\text{C}_3\text{H}_5(\text{OH})_3$.

The IMPS spectra cross the real axis in the low frequency (LF) region at a photocurrent density I_1 and in the medium frequency region at a photocurrent density I_2 . I_1 is the steady-state photocurrent, while I_2 is the charge carrier generation current [34]. The generation current expressed in electrical units is the flux of photoexcited minority charge carriers from the bulk of the semiconductor to its surface (i.e., the photocurrent in the absence of surface recombination of holes). Figure 9 shows the IMPS spectra normalized to I_2 . The point of intersection of the normalized IMPS spectrum with the real axis in the LF region corresponds to I_1/I_2 and shows the fraction of recombination losses during the electrocatalytic oxidation of depolarizers. It is seen from Figure 9 that significant surface recombination of photogenerated electron-hole pairs is observed in aqueous solution of 0.1 M KOH. At a potential of 0.4 V, the photocurrent makes 28% and the recombination loss is 72% of the hole generation current. It can also be seen from Figure 9 that the introduction of 20% CH_3OH into 0.1 M KOH aqueous solution reduces the recombination losses at the photoanode from 72 to 16%. This results from the principal role of photoinduced holes in the process of photoelectro-oxidation of CH_3OH molecules. The introduction of 20% $\text{C}_2\text{H}_4(\text{OH})_2$ or $\text{C}_3\text{H}_5(\text{OH})_3$ into the solution reduces the recombination losses in the photoanode almost down to zero (Figure 9, curves 3 and 4). Thus, these depolarizers are more efficiently oxidized by photogenerated holes than water and CH_3OH molecules.

From the normalized IMPS data, the recombination rate constant K_{rec} and charge transfer rate constant K_{ct} were calculated. The LF limit of the normalized IMPS in Figure 9, equal to I_1/I_2 , is related to the rate constants of recombination and charge transfer as $I_1/I_2 = K_{\text{ct}}/(K_{\text{rec}} + K_{\text{ct}})$. The light modulation frequency on the photoanode corresponding to the maximum of the semicircle located in the first quadrant f_{max} allows one to find the sum $(K_{\text{rec}} + K_{\text{ct}})$ using the equation: $2\pi f_{\text{max}} = (K_{\text{rec}} + K_{\text{ct}})$. The values of K_{rec} and

K_{ct} calculated from these two ratios for the processes of photoelectro-oxidation of water, methanol, and glycerol are given in Table 1. It can be seen that the chemical nature of the depolarizer affects both constants. A significant increase in K_{ct} is observed in the series $H_2O < CH_3OH < C_3H_5(OH)_3$. The accelerated consumption of holes entering the surface states of the photoanode in the photoelectro-oxidation of methanol and glycerol, in turn, decreases K_{rec} in the series $H_2O > CH_3OH > C_2H_4(OH)_2 \approx C_3H_5(OH)_3$. A comparison of Figures 6 and 9 shows that an increase in the photocurrent in the case of $C_2H_4(OH)_2$ and $C_3H_5(OH)_3$ substrates compared to CH_3OH is associated not only with complete suppression of the recombination due to the rapid transfer of holes to the depolarizer, but also with an increase in the density of surface states of the photoanode due to the adsorption of $C_2H_4(OH)_2$ and $C_3H_5(OH)_3$ at the electrode/solution interface.

Table 1. Charge transfer and recombination constants at $E = 0.4$ V vs. Ag on film photoanode $Ti^{4+}/Fe_2O_3/FTO$ under monochromatic illumination at 452 nm, with a 14 mW cm^{-2} power density in aqueous solutions of 0.1 M KOH, 0.1 M KOH + 20% CH_3OH , and 0.1 M KOH + 20% $C_3H_5(OH)_3$.

| | K_{ct}, s^{-1} | K_{rec}, s^{-1} |
|----------------|-------------------------|--------------------------|
| H_2O | 10.8 | 27.8 |
| CH_3OH | 32.4 | 10.8 |
| $C_2H_4(OH)_2$ | $K_{tr} \gg K_{rec}$ | - |
| $C_3H_5(OH)_3$ | $K_{tr} \gg K_{rec}$ | - |

2.4. Photoelectrocatalytic Oxidation of 5,6,7,8-tetrahydro-2-naphthol

Estrone, 17β -estradiol, estriol, and 17α -ethinylestradiol, endocrine disruptors, are major contributors to estrogenicity in aquatic systems. These compounds have been found in broad range of natural and industrial waters [35]. Disinfection of drinking water requires reduction of the estrogenic activity of 17α -ethinylestradiol, a hormonal contraceptive drug. Ozone with an oxidation potential of 2.07 V was used for this purpose [36]. Photodegradation of estrogenic steroid hormones has also been described, and dispersed titanium dioxide was shown to exhibit the highest photocatalytic activity under ultraviolet irradiation. Photocatalytic degradation generally eliminates or reduces estrogenic activity, although some intermediates exhibit higher estrogenic activity than that of precursor steroid hormones. The retention of estrogenic activity is mainly associated with the presence of a phenolic fragment in the intermediates [37]. Here, 5,6,7,8-tetrahydro-2-naphthol is a model compound for evaluating the possibility of degradation of the reactive phenolic moiety in steroid hormones.

Figure 10 shows the polarization curve of the photoelectrochemical process occurring on a $Ti^{4+}/Fe_2O_3/FTO$ film photoanode in a background 0.1 M KOH electrolyte containing 5,6,7,8-tetrahydro-2-naphthol (curve 3). A well-pronounced wave of direct photoelectrochemical oxidation of 5,6,7,8-tetrahydro-2-naphthol is observed in the potential range 0–0.7 V vs. Ag. It can be assumed that at higher potentials this substance will also be subject to oxidation by the $OH\bullet$ radicals formed during the photoelectro-oxidation of water, the potential of which (2.06 V) [38] is also sufficient to oxidize the substrate. Composition of the degradation products is very complex and is the subject of ongoing research.

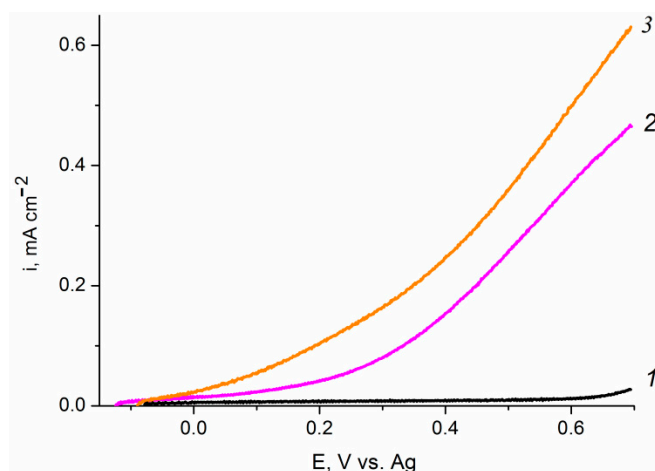


Figure 10. Polarization curves of a $\text{Ti}^{4+}/\text{Fe}_2\text{O}_3/\text{FTO}$ film photoanode measured: (1) in dark conditions, and (2, 3) under visible light illumination with a power density of 100 mW cm^{-2} in aqueous solutions of 0.1 M KOH and 0.1 M KOH + 0.01 mM 5,6,7,8-tetrahydro-2-naphthol, respectively.

2.5. Estimation of Recombination Losses during Photoelectro-Oxidation of 5,6,7,8-tetrahydro-2-naphthol

Comparison of Figures 6 and 10 shows that the electro-oxidation photocurrent density in the presence of 5,6,7,8-tetrahydro-2-naphthol is higher than in 0.1 M KOH solution, but it is approximately two times lower than the photocurrent density of methanol electro-oxidation from 0.1 M KOH + 20% CH_3OH solution. Together with the data from Figure 9 this indicates the presence of significant recombination losses during the photoelectrocatalytic oxidation of 5,6,7,8-tetrahydro-2-naphthol at a photoanode potential of 0.4 V vs. Ag. The same is also evidenced by the shape of the photocurrent transients shown in Figure 11.

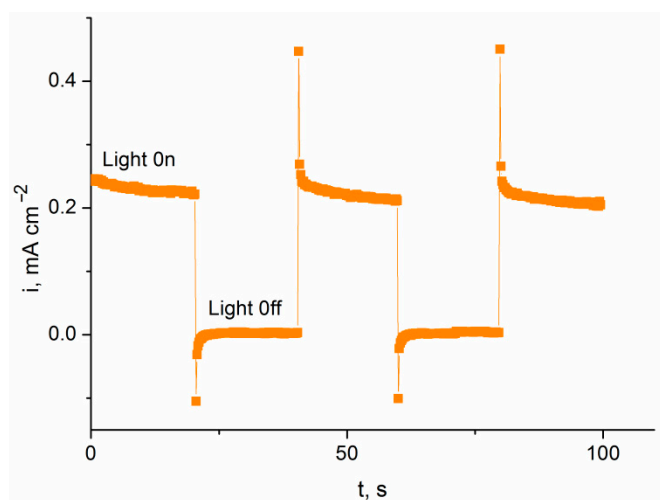


Figure 11. Photocurrent transients of a $\text{Ti}^{4+}/\text{Fe}_2\text{O}_3/\text{FTO}$ film photoanode measured in an aqueous solution of 0.1 M KOH + 0.01 mM 5,6,7,8-tetrahydro-2-naphthol at $E = 0.4 \text{ V}$ in dark conditions and under visible light illumination with a power density of 100 mW cm^{-2} .

It can be seen that turning the light “on” and “off” at a potential of 0.4 V leads to sharp jumps in the photocurrent, which rapidly drop to a stationary value due to the recombination of photogenerated electron-hole pairs during simultaneous photoelectrocatalytic oxidation of 5,6,7,8-tetrahydro-2-naphthol and water molecules. Figure 12 compares the normalized IMPS spectra for a $\text{Ti}^{4+}/\text{Fe}_2\text{O}_3/\text{FTO}$ film photoanode in the background solution and in the presence of 5,6,7,8-tetrahydro-2-naphthol. It can be seen that the addition of 0.01 mM 5,6,7,8-tetrahydro-2-naphthol to 0.1 M KOH leads to a decrease in recombination losses from 72 to 59 %. The values of K_{ct} and K_{rec} calculated from the IMPS data are

15.8 s^{-1} and 22.8 s^{-1} , respectively. The results obtained, together with the data in Table 1 imply the dominant role of photoinduced holes in the process of photoelectro-oxidation of 5,6,7,8-tetrahydro-2-naphthol molecules compared to water molecules.

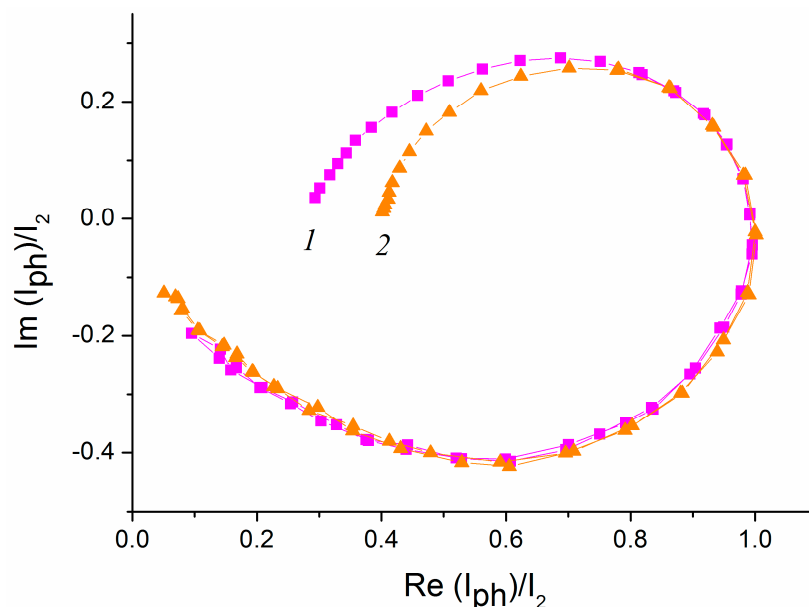


Figure 12. Normalized IMPS spectra for a $\text{Ti}^{4+}/\text{Fe}_2\text{O}_3/\text{FTO}$ film photoanode illuminated with monochromatic light 452 nm at illumination power density 14 mW cm^{-2} obtained at a potential of 0.4 V in aqueous solutions of (1) 0.1 M KOH and (2) 0.1 M KOH + 0.01 mM 5,6,7,8-tetrahydro-2-naphthol.

3. Experimental Section

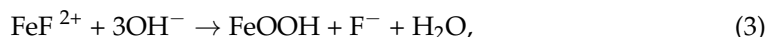
3.1. Materials

Chemically pure (>99%) ferric chloride ($\text{FeCl}_3 \cdot 6\text{H}_2\text{O}$), potassium fluoride ($\text{KF} \cdot 2\text{H}_2\text{O}$), and potassium chloride (KCl), titanium tetra n-butoxide ($\text{Ti}(\text{OBU})_4$), 35% hydrogen peroxide (H_2O_2), purchased from Aldrich (Burlington, MA, USA) and used in the film coating fabrication without further purification. To manufacture the photoanodes, glass with an electrically conductive coating (specific resistance $\approx 7 \Omega \text{ cm}^{-2}$) of fluorine-stabilized tin dioxide (F: SnO_2 , FTO) (Aldrich) was used.

3.2. Preparation of Hematite and Doped Hematite Films

Polycrystalline $\alpha\text{-Fe}_2\text{O}_3$ photoanodes were formed on FTO-coated glass substrates. The substrate was preliminarily cleaned by ultrasonication in acetone, isopropanol, and distilled water baths (15 min in each one). The cleaned glass substrate was fixed in a Teflon frame so that the surface to be coated was 1 cm^2 , the uncoated part of the sample was fixed in a titanium current lead, and a three-electrode system was assembled on a Teflon cover. A Pt–Ir alloy plate (Ir content 10%) with 8 cm^2 area was used as an anode, and a silver plate served as a reference electrode. The assembled block of electrodes was placed in a 100 mL thermostated cell equipped with a water jacket. The distance between the anode and the cathode was 3 cm. The electrochemical cell was filled with an electrolyte solution (12.5 mM FeCl_3 , 50 mM KF, 0.1 M KCl and 1 M H_2O_2) immediately before $\alpha\text{-Fe}_2\text{O}_3$ deposition. The hematite film was electrodeposited for 5 min under potentiostatic conditions at a potential of -0.35 V vs. Ag and a temperature of $70 \text{ }^\circ\text{C}$. The chronoamperometric curve was recorded using a PAR 273 potentiostat (Princeton Applied Research, Oak Ridge, TN, USA). The amount of electricity consumed during the deposition was 1.6–2.0 C. The reactions proceeding during electrodeposition are described in several works [39,40]:





and the overall reaction can be represented by the equation:



As a result of the electrodeposition, a yellow FeOOH film was obtained on the glass substrate. It was thoroughly washed with distilled water, dried at room temperature, and then annealed in air in a tube furnace at 500 °C for 2 h. Then the temperature in the furnace was raised to 750 °C for additional treatment for 10 min. After cooling in the furnace for 12 h, the resulting samples with a uniform red α -Fe₂O₃ film ~600–800 nm thick were obtained.

3.3. Modification of Hematite Films

To prepare photoanodes with modified hematite, first a hematite film was obtained according to the method described in the previous subsection. Then 0.05 mL tetrabutoxytitanium (Ti(OBu)₄) was applied to the formed α -Fe₂O₃ film coating by spin-coating with the sample rotating at 2000 rpm. After drying, the sample was calcined at 500 °C for 2 h and then at 750 °C for 10 min (ramp rate 10 deg/min).

3.4. Characterization of the Samples

The phase composition of the photoelectrocatalytic film coatings was studied by X-ray diffraction (XRD) analysis on an Empyrean X-ray diffractometer (Panalytical BV, Almelo, Netherlands). Ni-filtered Cu-K α radiation was used; the samples were studied in the Bragg–Brentano geometry. Experimental diffraction patterns were processed using the Highscore program; the phase composition was identified using the ICDD PDF-2 diffraction database. The average size of crystallites of the identified phase was determined from the broadening of the observed diffraction peaks using Williamson–Hall and Scherrer methods. The spectral characteristics of the obtained films were studied in a range of 300–1100 nm at room temperature using a Lambda35 Perkin Elmer spectrometer. Raman spectra were recorded using an inVia “Reflex” Raman spectrometer (Renishaw, New Mills Wotton-under-Edge UK) with 633 nm excitation wavelength and laser power on the sample less than 0.2 mW; 20 \times objective.

3.5. Photoelectrochemical Measurements

For photoelectrochemical studies a setup consisting of a PECC-2 photoelectrochemical three-electrode cell (Zahner Elektrik, Kronach, Germany), a solar spectrum simulator 96000 (Newport, Irvine NV, USA) with an AM1.5G filter and a power of 150 W, and an IPC-Pro MF potentiostat (IPCE RAS, Moscow, Russia) was used. The working electrode in the cell was a photoanode made of hematite or hematite doped with titanium in the form of a film coating with a surface area of 1 cm². A platinum wire with a surface area of \approx 3 cm² served as the auxiliary electrode. A silver wire was used as a reference electrode, relative to which all potentials are given in this work. Illumination was carried out from the reverse side of the photoanode, and the illumination power at different distances from the light source was determined using a Nova instrument (OPHIR-SPIRICON Inc., Jerusalem, Israel). Photoelectrochemical oxidation of organic substrates on prepared photoanodes was carried out under visible light illumination (1 sun) at a power density of 100 mW cm⁻². The IMPS spectra of the photocurrent were recorded on a computerized photoelectrochemical station Zahner PP 211 CIMPS (Zahner-Elektrik) GmbH & Co.KG, Kronach, Germany) in the frequency range from 1000 to 0.02 Hz. The station was equipped with a TLS03 monochromatic light source with a set of LEDs with wavelengths from 320 to 1020 nm and the CIMPS-QE/IPCE software package. The IMPS spectra were recorded under the illumination of a photoanode with monochromatic light with a wavelength of λ = 452 nm

and a fixed intensity of 14 mW cm^{-2} . A sinusoidal disturbance (~10% of stationary illumination) was superimposed on a constant base light intensity.

4. Conclusions

The results of the study show that modification of the surface of an electrodeposited thin-film hematite photoelectrode with a small amount of titanium leads to a significant intensification of the processes of photoelectrocatalytic degradation of alcohols with various structures. This modification of the hematite surface increases the efficiency of charge transfer through the photoanode/solution interface upon illumination with a sunlight simulator. Since alcohol substrate molecules in a 0.1 M KOH solution are more effective acceptors of photoinduced holes compared to water molecules, they suppress recombination processes on the surface of modified photoanodes. The increase in the photoelectro-oxidation rate in the series $\text{H}_2\text{O} < \text{CH}_3\text{OH} < \text{C}_2\text{H}_4(\text{OH})_2 < \text{C}_3\text{H}_5(\text{OH})_3$ can be explained by the influence of the chemical nature of the depolarizer on both the photoelectro-oxidation rate constant transfer of holes to the depolarizer and the recombination processes on the surface states of the titanium-promoted hematite photoanode.

Thus, it has been shown that the chemical nature of the depolarizer plays an important role in increasing the efficiency of charge separation and the charge transfer rate constant during the photoelectrocatalytic oxidation of some alcohols. It has also been shown that the modification of $\alpha\text{-Fe}_2\text{O}_3$ with titanium provides maximum activity of the photoanode with respect to the reaction of photoelectro-oxidation of glycerol from an aqueous solution.

Author Contributions: V.A.G.: General conceptualization and preparation of film photoanodes. V.V.E.: preparation of photoanodes and IMPS investigation. N.A.M.: photoelectrochemical measurements. A.A.A.: UV and Raman spectroscopic measurements. A.A.S.: XRD and X-ray fluorescence studies. All authors have read and agreed to the published version of the manuscript.

Funding: This research received no external funding.

Data Availability Statement: Not applicable.

Acknowledgments: The research was performed according to the IPCE RAS state assignment using the equipment of the Center for Collective Use of Physical Investigation Methods of the IPCE RAS.

Conflicts of Interest: The authors declare that they have no known competing financial interests or personal relationships that could have appeared to influence the work reported in this paper.

References

1. Dodekatos, G.; Schünemann, S.; Tüysüz, H. Recent advances in thermo-, photo-, and electrocatalytic glycerol oxidation. *ACS Catal.* **2018**, *8*, 6301–6333. [[CrossRef](#)]
2. Tan, H.W.; Abdul Aziz, A.R.; Aroua, M.K. Glycerol production and its applications as a raw material: A review. *Renew. Sustain. Energy Rev.* **2013**, *27*, 118–127. [[CrossRef](#)]
3. Sun, D.; Yamada, Y.; Sato, S.; Ueda, W. Glycerol as a potential renewable raw material for acrylic acid production. *Green Chem.* **2017**, *19*, 3186–3213. [[CrossRef](#)]
4. Dusselier, M.; Van Wouwe, P.; Dewaele, A.; Makshina, E.; Sels, B.F. Lactic acid as a platform chemical in the biobased economy: The role of chemocatalysis. *Energy Environ. Sci.* **2013**, *6*, 1415–1442. [[CrossRef](#)]
5. Razali, N.; Abdullah, A.Z. Production of lactic acid from glycerol via chemical conversion using solid catalyst: A review. *Appl. Catal. A Gen.* **2017**, *543*, 234–246. [[CrossRef](#)]
6. Ciriminna, R.; Palmisano, G.; Della Pina, C.; Pagliaro, M. One-pot electrocatalytic oxidation of glycerol to DHA. *Tetrahedron Lett.* **2006**, *47*, 6993–6995. [[CrossRef](#)]
7. Pagliaro, M.; Ciriminna, R.; Kimura, H.; Rossi, M.; Della Pina, C. From glycerol to value-added products. *Angew. Chemie Int. Ed.* **2007**, *46*, 4434–4440. [[CrossRef](#)] [[PubMed](#)]
8. Katryniok, B.; Kimura, H.; Skrzyńska, E.; Girardon, J.-S.; Fongarland, P.; Capron, M.; Ducoulombier, R.; Mimura, N.; Paul, S.; Dumeignil, F. Selective catalytic oxidation of glycerol: Perspectives for high value chemicals. *Green Chem.* **2011**, *13*, 1960–1979. [[CrossRef](#)]
9. Gan, W.Y.; Friedmann, D.; Amal, R.; Zhang, S.; Chiang, K.; Zhao, H. A comparative study between photocatalytic and photoelectrocatalytic properties of Pt deposited TiO_2 thin films for glucose degradation. *Chem. Eng. J.* **2010**, *158*, 482–488. [[CrossRef](#)]
10. Lu, X.; Xie, S.; Yang, H.; Tong, Y.; Ji, H. Photoelectrochemical hydrogen production from biomass derivatives and water. *Chem. Soc. Rev.* **2014**, *43*, 7581–7593. [[CrossRef](#)]

11. Pawar, A.U.; Kim, C.W.; Kang, M.J.; Kang, Y.S. Crystal facet engineering of ZnO photoanode for the higher water splitting efficiency with proton transferable nafion film. *Nano Energy* **2016**, *20*, 156–167. [[CrossRef](#)]
12. Liu, H.; Lv, T.; Zhu, C.; Su, X.; Zhu, Z. Efficient synthesis of MoS₂ nanoparticles modified TiO₂ nanobelts with enhanced visible-light-driven photocatalytic activity. *J. Mol. Catal. A Chem.* **2015**, *396*, 136–142. [[CrossRef](#)]
13. Lee, Y.; Kim, S.; Jeong, S.Y.; Seo, S.; Kim, C.; Yoon, H.; Jang, H.W.; Lee, S. Surface-Modified Co-doped ZnO Photoanode for Photoelectrochemical Oxidation of Glycerol. *Catal. Today* **2021**, *359*, 43–49. [[CrossRef](#)]
14. Bessegato, G.G.; Guaraldo, T.T.; Zanoni, M.V.B. Enhancement of photoelectrocatalysis efficiency by using nanostructure electrodes. In *Modern Electrochemical Methods in Nano, Surface and Corrosion Science*; Aliokhazraei, M., Ed.; IntechOpen: London, UK, 2014; Chapter 10; pp. 271–320.
15. Peleyeju, M.G.; Arotiba, O.A. Recent trend in visible-light photoelectrocatalytic systems for degradation of organic contaminants in water/wastewater. *Environ. Sci. Water Res. Technol.* **2018**, *4*, 1389–1411. [[CrossRef](#)]
16. Mishra, M.; Chun, D. α -Fe₂O₃ as a photocatalytic material: A review. *Appl. Catal. A Gen.* **2015**, *498*, 126–141. [[CrossRef](#)]
17. Zhang, M.; Pu, W.; Pan, S. Photoelectrocatalytic activity of liquid phase deposited α -Fe₂O₃ films under visible light illumination. *J. Alloys Compd.* **2015**, *648*, 719–725. [[CrossRef](#)]
18. Masoumi, Z.; Tayebi, M.; Kolaie, M.; Lee, B.K. Efficient and stable core-shell α -Fe₂O₃/WS₂/WO_x photoanode for oxygen evolution reaction to enhance photoelectrochemical water splitting. *Appl. Catal. B Environ.* **2022**, *313*, 121447. [[CrossRef](#)]
19. Masoumi, Z.; Tayebi, M.; Kolaie, M.; Tayyebi, A.; Ryu, H.; Jang, J.I.; Lee, B.-K. Simultaneous Enhancement of Charge Separation and Hole Transportation in a W: α -Fe₂O₃/MoS₂ Photoanode: A Collaborative Approach of MoS₂ as a Heterojunction and W as a Metal Dopant. *ACS Appl. Mater. Interfaces* **2021**, *13*, 39215–39229. [[CrossRef](#)] [[PubMed](#)]
20. Masoumi, Z.; Tayebi, M.; Lee, B.-K. The role of doping molybdenum (Mo) and back-front side illumination in enhancing the charge separation of α -Fe₂O₃ nanorod photoanode for solar water splitting. *Sol. Energy* **2020**, *205*, 126–134. [[CrossRef](#)]
21. Mesa, C.A.; Kafizas, A.; Francàs, L.; Pendlebury, S.R.; Pastor, E.; Ma, Y.; Le Formal, F.; Mayer, M.T.; Grätzel, M.; Durrant, J.R. Kinetics of Photoelectrochemical Oxidation of Methanol on Hematite Photoanodes. *J. Am. Chem. Soc.* **2017**, *139*, 11537–11543. [[CrossRef](#)]
22. Iervolino, G.; Tantis, I.; Sygellou, L.; Vaiano, V.; Sannino, D.; Lianos, P. Photocurrent increase by metal modification of Fe₂O₃ photoanodes and its effect on photoelectrocatalytic hydrogen production by degradation of organic substances. *Appl. Surf. Sci.* **2017**, *400*, 176–183. [[CrossRef](#)]
23. Grinberg, V.A.; Emets, V.V.; Mayorova, N.A.; Averin, A.A.; Tsodikov, M.V.; Maslov, D.A. Methanol Photoelectrooxidation on Hematite Films Modified with TiO₂, Bi, and Co. *Russ. J. Electrochem.* **2022**, *58*, 667–675. [[CrossRef](#)]
24. Liu, Y.; Wang, D.-P.; Yu, Y.-X.; Zhang, W.-D. Preparation and photoelectrochemical properties of functional carbon nanotubes and Ti co-doped Fe₂O₃ thin films. *Int. J. Hydrogen Energy* **2012**, *37*, 9566–9575. [[CrossRef](#)]
25. Cesar, I.; Kay, A.; Martinez, J.A.G.; Gratzel, M. Translucent thin film Fe₂O₃ photoanodes for efficient water splitting by sunlight: Nanostructure-directing effect of Si-doping. *J. Am. Chem. Soc.* **2006**, *128*, 4582–4583. [[CrossRef](#)]
26. Monllor-Satoca, D.; Bärtsch, M.; Fàbrega, C.; Gen, A.; Reinhard, S.; Andreu, T.; Arbiol, J.; Niederberger, M.; Morante, J.R. What do you do, titanium? Insight into the role of titanium oxide as a water oxidation promoter in hematite-based photoanodes. *Energy Environ. Sci.* **2015**, *8*, 3242–3254. [[CrossRef](#)]
27. Tauc, J.; Menth, A. State in the gap. *J. Non Cryst. Solids* **1972**, *8*, 569–585. [[CrossRef](#)]
28. Chakrabarti, M.; Dutta, S.; Chattapadhyay, S.; Sarkar, A.; Sanyal, D.; Chakrabarti, A. Grain size dependence of optical properties and positron annihilation parameters in Bi₂O₃ powder. *J. Nanotech.* **2004**, *15*, 1792–1796. [[CrossRef](#)]
29. Landolsi, Z.; Ben Assaker, I.; Chtourou, R.; Ammar, S. Photoelectrochemical impedance spectroscopy of electrodeposited hematite α -Fe₂O₃ thin films: Effect of cycle numbers. *J. Mat. Sci. Mater. Electron.* **2018**, *29*, 8176–8187. [[CrossRef](#)]
30. Peter, L.M.; Ponomarev, E.A.; Fermin, D.J. Intensity-modulated photocurrent spectroscopy: Reconciliation of phenomenological analysis with multistep electron transfer mechanisms. *J. Electroanal. Chem.* **1997**, *427*, 79–96. [[CrossRef](#)]
31. Peter, L.M.; Wijayantha, K.G.U.; Tahir, A.A. Kinetics of light-driven oxygen evolution at α -Fe₂O₃ electrodes. *J. Faraday Discuss.* **2012**, *155*, 309–322. [[CrossRef](#)]
32. Thorne, J.E.; Zhao, Y.; He, D.; Fan, S.; Vanka, S.; Mi, Z.; Wang, D. Understanding the Role of Co-Catalysts on Silicon Photocathodes Using Intensity Modulated Photocurrent Spectroscopy. *Phys. Chem. Chem. Phys.* **2017**, *19*, 29653–29659. [[CrossRef](#)]
33. Klotz, D.; Ellis, D.S.; Dotana, H.; Rothschild, A. Empirical in operando Analysis of the Charge Carrier Dynamics in Hematite Photoanodes by PEIS, IMPS and IMVS. *J. Phys. Chem. Chem. Phys.* **2016**, *18*, 23438–23457. [[CrossRef](#)]
34. Gartner, W.W. Depletion-Layer Photoeffects in Semiconductors. *Phys. Rev.* **1959**, *116*, 84–87. [[CrossRef](#)]
35. Onda, K.; Nakamura, Y.; Takatoh, C.; Miya, A.; Katsu, Y. The behavior of estrogenic substances in the biological treatment process of sewage. *Water Sci. Technol.* **2003**, *47*, 109–116. [[CrossRef](#)] [[PubMed](#)]
36. Huber, M.M.; Ternes, T.A.; Von Gunten, U. Removal of Estrogenic Activity and Formation of Oxidation Products during Ozonation of 17 α -Ethinylestradiol. *Environ. Sci. Technol.* **2004**, *38*, 5177–5186. [[CrossRef](#)] [[PubMed](#)]
37. Sornalingam, K.; McDonagh, A.; Zhou, J.L. Photodegradation of estrogenic endocrine disrupting steroidal hormones in aqueous systems: Progress and future challenges. *Sci. Total Environ.* **2016**, *550*, 209–224. [[CrossRef](#)]
38. Goswami, D.Y.; Kreith, F.; Kreider, J.F. *Principles of Solar Engineering*, 2nd ed.; Taylor & Francis, Co.: Philadelphia, PA, USA, 1999; pp. 448–455+694.

39. Phuana, Y.W.; Ongc, W.J.; Chonga, M.N.; Ocone, J.D. Prospects of electrochemically synthesized hematite photoanodes for photoelectrochemical water splitting: A review. *J. Photochem. Photobiol.* **2017**, *33*, 54–82. [[CrossRef](#)]
40. Schrebler, R.; Bello, K.; Vera, F.; Cury, P.; Muñoz, E.; Río, R.D.; Meier, H.G.; Órdova, R.C.; Dalchiele, E.A. An electrochemical deposition route for obtaining α -Fe₂O₃ thin films. *Electrochem. Solid State Lett.* **2006**, *9*, 110–113. [[CrossRef](#)]